Ex-situ characterisation of water droplet dynamics on the surface of a fuel cell gas diffusion layer through wettability analysis and thermal characterisation

Oluwamayowa A. Obeisun[1], Donal P. Finegan[1,2], Erik Engebretsen[1,2], James B. Robinson[1], Damilola Taiwo[1], Gareth Hinds[2], Paul Shearing[1] and Daniel J. L. Brett[1]*

[1]Electrochemical Innovation Lab, Department of Chemical Engineering, University College London, WC1E 7JE, London United Kingdom

[2] National Physical Laboratory, Hampton Rd., Teddington, Middlesex, TW11 0LW, UK

Keywords: Contact angle; water droplet; gas diffusion layer; thermal imaging; X-ray computed tomography.

* Author to whom correspondence should be addressed

Tel.: +44(0)20 7679 3310

Web: www.ucl.ac.uk/electrochemical-innovation-lab

Email: d.brett@ucl.ac.uk

Abstract

Understanding the evaporation of water from gas diffusion layers (GDL) is important for polymer electrolyte fuel cell (PEFC) design and operational purposes, particularly for open-cathode air-breathing fuel cells where water removal is purely through evaporation. In this work, water droplet dynamics on the surface of a fuel cell GDL is studied by wettability and thermal characterisation. The droplet maintains a fixed contact diameter (pinned) until there is a transition from non-wetting to wetting regime, after which the contact diameter reduced rapidly until complete evaporation occurs. GDL thermal characterisation reveals that temperature variation encountered across the GDL is due to a change in emissivity and increased thermal gradient across the GDL due to its uneven surface. Droplet thermal characterisation reveals that the droplets have a cooling effect on the surrounding GDL when introduced at room temperature and the cooling effect is more exacerbated with an increase in GDL temperature. This work provides insight into the dynamics of water evaporation on GDLs which could be effective in developing water and heat management strategies in PEFCs, as water droplets are expected to experience similar pinning and cooling effect to that observed in this work within the cathode gas channels of PEFCs. This is particularly relevant to passive open-cathode cells.

1 Introduction

Polymer electrolyte fuel cells (PEFCs) are a promising alternative power generation technology due to their high energy conversion efficiency, low temperature operation and high power density [1]. Open-cathode air-breathing fuel cells are attractive for portable power applications, as in passive mode they do not require forced convection of air to the cathode, so avoiding the need for blowers and reducing balance-of-plant requirements [2]. In air-breathing fuel cells, the cathode is exposed to the atmosphere and supply of oxygen is achieved through free or natural convection of air [3,4].

Effective water management is one of the greatest technological challenges for PEFC commercialisation [5]. Water is required to hydrate the electrolyte for improved proton conductivity and transport of water occurs across the membrane through hydraulic gradients [6]. However, excess water can fill open pores in the GDL which can act to block reactant access to the catalyst [7]. This phenomenon is known as 'flooding' and can significantly diminish fuel cell performance, particularly at high current density. Introducing a hydrophobic content to the GDL helps to avoid water build-up within open pores; however, as a result of this, water droplets can readily form on the surface of the GDL. Understanding how these droplets form and evaporate is important for design and operational optimisation.

In conventional closed cathode fuel cells, the propensity of liquid water to be removed from the surface of the GDL is strongly influenced by superficial gas velocity [8]. For high superficial gas velocity, the shear force from the gas flow detaches droplets from the GDL surface. Lower gas velocity allows droplets to grow in size until they touch hydrophilic channel walls and spread. However, in open-cathode fuel cells, water removal is purely by evaporation due to lack of forced convection mechanism; in which case, current density and temperature plays the major role in determining how droplets form and evaporate.

Various experimental techniques have been reported showing how liquid water is transported and distributed in PEFCs. Techniques such as NMR imaging [9–11] and beam interrogation techniques, such as neutron imaging [12–16] and X-ray imaging [17–19] enable the *in situ* measurement of liquid water distribution in operating PEFCs. However, such techniques are costly, require advanced imaging facilities and are often limited by spatial and temporal resolutions which are required for dynamic in-situ studies. Direct optical visualisation [20–22] has proven to be a powerful technique for observing water droplet formation, motion and evaporation in operating fuel cells [23–26]. The technique benefits

from high spatial and temporal resolution and depending on the optical set-up, direct access to the surface of the GDL is enabled (such as in the case of an open-cathode fuel cell).

Water visualisation work on GDLs has mainly focused on liquid water formation and transport [7,8,15,21,22,27] with little work has been done on evaporation. Work reported to date indicates that droplet detachment and growth in PEFCs is highly dependent on the superficial gas velocity [7,8,15,21,22,27] and droplet 'pinning'[7,8]. A droplet is considered 'pinned' when it doesn't easily detach from the GDL surface and the contact line along the liquid water-GDL interface does not change [8]. Pinning is influenced by superficial air velocity, surface roughness and structure [8].

Though all these studies have provided useful results in the understanding of droplet behaviour in PEFCs, the results are mainly only applicable to conventional fuel cells, which utilise forced convection of air to the cathode. In open-cathode fuel cells, droplet detachment from the GDL is purely by evaporation as there is no forced convection of air to the cathode, meaning gas velocity does not play a role in detaching droplets, although free-convection induced by temperature gradients and buoyancy forces may be a factor. This presents an interesting area of study – visualisation and study of droplet evaporation dynamics on a fuel cell GDL.

In open-cathode fuel cells, drying of the membrane has been identified to be one of the major sources of limiting current density [28]. Therefore, an understanding of the dynamics of droplet evaporation on GDLs can be useful in developing droplet heat and water management strategies which can be effective at moderating PEFC temperature.

Despite there being little work reported on droplet evaporation from GDLs, some work has been done on droplet evaporation from hydrophobic surfaces that we can learn from. Droplet evaporation depends on surface wettability [29], contact angle hysteresis [30] and surface roughness [31]. Picknett and Bexon [32] identified two modes of evaporation for a droplet resting on a smooth hydrophobic surface, namely the constant contact angle (CCA) mode and the constant contact radius (CCR) mode. During the CCA mode, the contact angle is unchanged during evaporation, the drop shape remaining that of a spherical cap, but with diminishing area of contact between liquid and surface [32]. During the CCR mode, evaporation takes place with unchanged contact area between liquid and surface, the shape remaining that of a spherical cap, but with diminishing contact angle. Evaporation was observed to begin in the CCR mode before transitioning to the CCA mode [32].

Hao *et al.* [33] studied the evaporating behaviour of water droplets on superhydrophobic surfaces. Their results revealed that the receding contact angle of water droplets increased during evaporation. McHale *et al.* [34] reported that droplet evaporation on superhydrophobic surfaces follows three modes: a CCR mode, a CCA mode and a mixed mode in which they both decrease simultaneously. Dash *et al.* [35] studied the evaporation characteristics of water droplets on heated hydrophobic and superhydrophobic surfaces and their results revealed that evaporation is purely in CCA mode as the droplet radius constantly reduced. While work has been done on droplet evaporation on hydrophobic and superhydrophobic surfaces, most of the characterisation work performed has been limited to studying its wettability characteristics on different surfaces. However, in this study, thermal visualisation and characterisation of a droplet's evaporating dynamics is used in combination with wettability studies. This is particularly important as thermal imaging is being increasingly used for fuel cell diagnostics and the characterisation performed will help interpretation of droplet shape and form from infrared measurements during fuel cell operation.

Thermal characterisation / mapping is a powerful diagnostic tool for the study of fuel cells [36–41]. Knowledge of temperature distribution on the MEA surface of PEFCs is very important as it affects localised current density, water and thermal management. Thermal imaging can help identify the location of hotspots, which can accelerate degradation and eventual failure of the membrane [42–44] and in the design of different fuel cell cooling systems [45–48].

The paper describes a comprehensive characterisation of the dynamics of water droplet evaporation from the surface of gas diffusion layers used in polymer electrolyte fuel cells. Water droplet behaviour of GDLs plays an important role electrode flooding and heat rejection from fuel cells. For the first time, this work describes droplet evaporation based on droplet form and shape as well as its thermal signature. Important insight into the evaporation dynamics is realised, this is correlated with the thermal response and some important new insights with regard to studying fuel cells using thermal imaging cameras are identified.

2 Experimental

The GDL used for characterisation was a commercially available Toray carbon fibre paper (Toray Industries, Inc. product code TGP-H-030). The GDL wettability characterisation was performed using an optical DSA100 drop shape analysis system (KRUSS GmbH, Hamburg). Drop shape analysis (DSA) is an image analysis method for determining the contact angle from the shadow image of a sessile drop and the surface tension or interfacial tension from the shadow image. The system uses a diffuse backlight to illuminate the drop; this provides high contrast between the edge of the droplet and its surroundings. The contact angle was calculated using sessile drop fitting or the Young-Laplace technique [49], which assumes the effect of gravity to be negligible. The drop image is illuminated from one side and a high resolution CCD camera at the opposite side records an image of the drop. The drop image is transferred to a computer equipped with a video-digitizer board (frame-grabber). The DSA software contains time-proven tools for analysing the drop image which can be used to calculate the contact angle. Evolution of the droplet-GDL contact angle during the evaporation process was done automatically by the DSA100. The DSA software detected the liquid-air interface through the liquid-solid-air contact point. The contact angle is between this tangent and the plane of the solid surface. A diagram of the setup is shown in Figure 1. Repeated measurements for each temperature resulted in contact angle measurements within $\pm 3^{o}$. An 8 µl ± 0.1 µl volume of deionised water was used for each droplet. The experiment was performed at room temperature which was recorded at 23 ºC. The relative humidity was measured at 40%. The experiments were performed on the same day and there was no change in the conditions. The temperature of the GDL was controlled by a hot plate over the range of 30 ^{o}C to 60 ^{o}C. This temperature range was chosen due to the temperature profiles achieved during thermal characterisation of the open-cathode fuel cell.

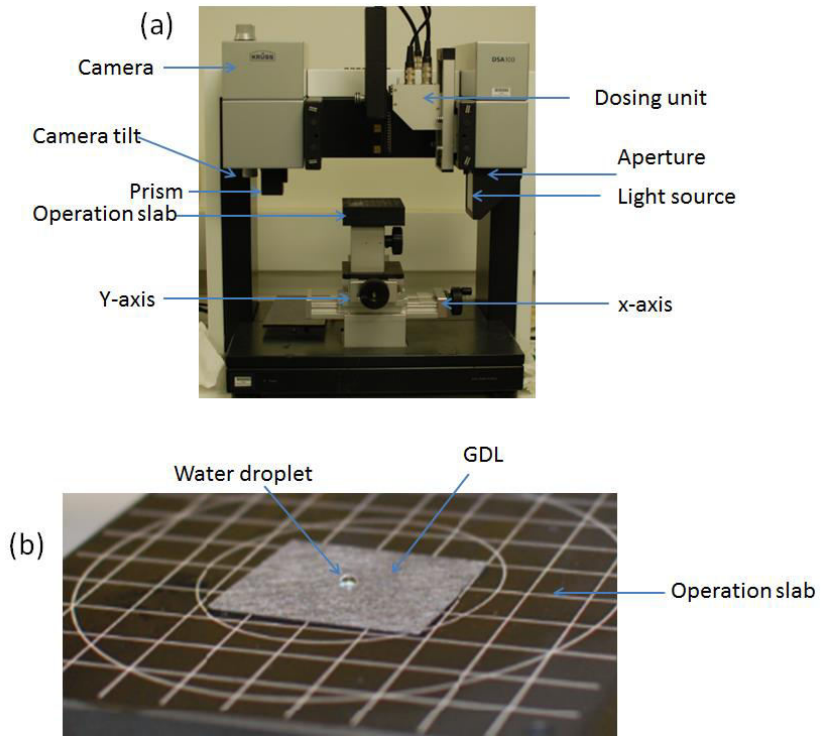

Figure 1 Experimental set up and label of the DSA100 equipment used for contact angle measurement; (b) focus on the operation slab with GDL and water droplet.

While injecting the droplet through the GDL (bottom injection) more accurately depict how water is formed in fuel cells i.e. from the catalyst layer and through to the GDL, injecting the droplet directly on top of the GDL enabled the wide range of studies conducted to be consistent, uniform and comparable. The temperature ranges would be difficult to achieve and may not be accurate. Since this paper targets open cathode fuel cells where droplet removal is purely by evaporation due to temperature changes, it was therefore important to keep the temperature factor.

Furthermore, Das et al [50], compared the bottom injection method to the top injection method by measuring the contact angle and adhesion force. They reported that while the contact angles and droplet contact diameter were different (larger with bottom injection), they followed the same trend during evaporation. They attributed this to the significant

water/water interaction created by the bottom injection which is likely to increase the droplet's adhesion (hence a larger contact diameter and angle).

Thermal imaging was performed using a 640 × 512 focal plane array InSb camera (SC5600MB FLIR, UK). The camera was calibrated for the temperature range in question (15 – 100 °C) with the images being recorded using commercially available software (ResearchIR, FLIR ATC, Croissy-Beaubourg, France).

X-ray CT of a section of the GDL was performed at the TOMCAT beamline at the Swiss Light Source (SLS). 1501 projections were acquired under a monochromatic 10.5 keV beam. The projections were reconstructed using a filtered back projection algorithm into a 3D image with a voxel size of 0.65 µm. The tomography image was binarized using Avizo Fire's Watershed algorithm, segmented using Avizo Fire's segmentation editor and saved as a surface (ASCII .stl) which was imported into Star CCM+ (CD-adapco) for polyhedral meshing. The volume was prepared in a similar way to that described by Cooper *et al.* [51].

3 Result and discussion

Images of the evaporating water droplet on the GDL surface are shown in Figure 2. Each column shows successive stages in the evaporation of the droplet with time at different temperatures. The images are taken from the side of the droplet and a reflection artefact is noticeable and associated with the white light illumination source. The evaporation time varies from 1450 s at 30 ^{o}C to 290 s at 60 ^{o}C.

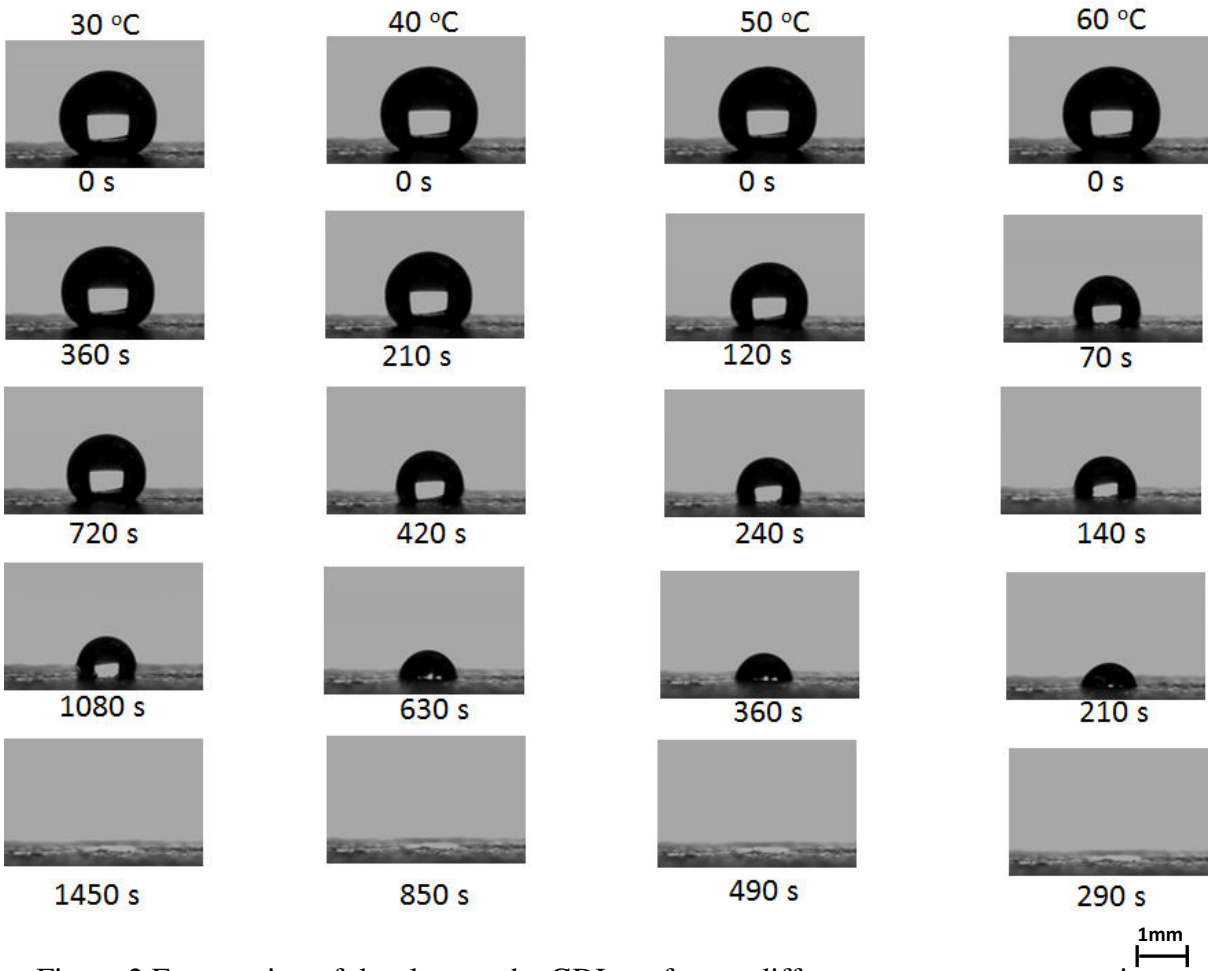

Figure 2 Evaporation of droplets on the GDL surface at different temperatures over time.

3.1 Effect of PTFE content on contact angle

The transport of liquid water through the GDL is not only reliant on pore structure, porosity and permeability but also degree of hydrophobicity of the GDL [52]. The contact angle the droplet (at different temperature) makes with GDLs of various PTFE contents was evaluated. The GDLs were commercially available Toray carbon fibre paper produced by Toray Industries. It should be noted that changing the temperature of the water bath regulated temperature of the droplet. However, when water is sucked into the syringe from the water bath and dropped onto the GDL the temperature would have reduced. However, for the purpose of comparison it is assumed that there is no reduction in droplet temperature when sucked out of the water bath. The GDL was at room temperature (20 $^{\circ}$C). The experiment was repeated three times over three different GDL samples of the same PTFE content with the average contact angle recorded. The result is displayed in Figure 3.

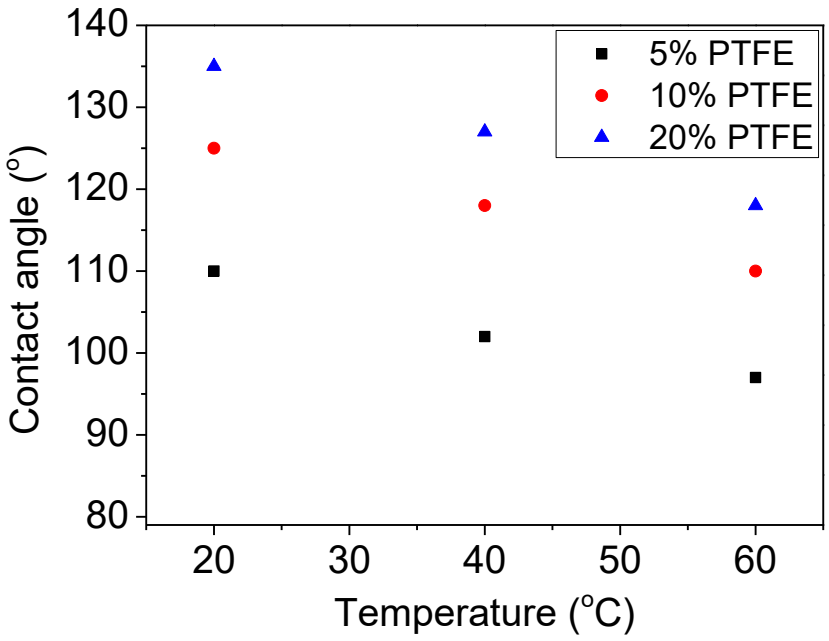

Figure 3 Evolution of droplet contact angle at different droplet temperature using GDLs coated with various amount of PTFE.

The data from Figure 3 shows that an increase in the PTFE content of GDL leads to an increase in the contact angle, which means a higher degree of hydrophobicity of the material. Fuel cells require the GDL to have a high degree of hydrophobicity to help with water management. It should be noted that a GDL's treatment with PTFE increases its thickness, reduces pores size and leads to higher contact resistance. Therefore, the PTFE content within the GDL cannot be increased indefinitely. Furthermore, it can be seen from Figure 3 that an

increase in temperature of the droplet leads to decrease in contact angle. This is expected because liquid-gas surface tension is affected by temperature. As temperature increases, surface tension decreases, and vice versa. An increase in temperature will therefore lead to a decrease in contact angle. The GDL with 20% PTFE was therefore used to study water droplet dynamics during evaporation.

3.1.1 Variation of contact angle, contact diameter and droplet diameter

The evolution of contact angle as liquid evaporates is shown in Figure 4a. The relative time change is also displayed in Figure 4b. The water droplet makes a large initial contact angle (130 ± 2^{o}) with the GDL for each of the different temperatures. This is within the range of studies describing contact angles on GDLs, which report values between 115 ° and 140 ° [53]. The initially high contact angle (hydrophobic surface) is indicative of the fact that the GDL is impregnated with PTFE, added to improve water management by expelling liquid water from the GDL structure [5].

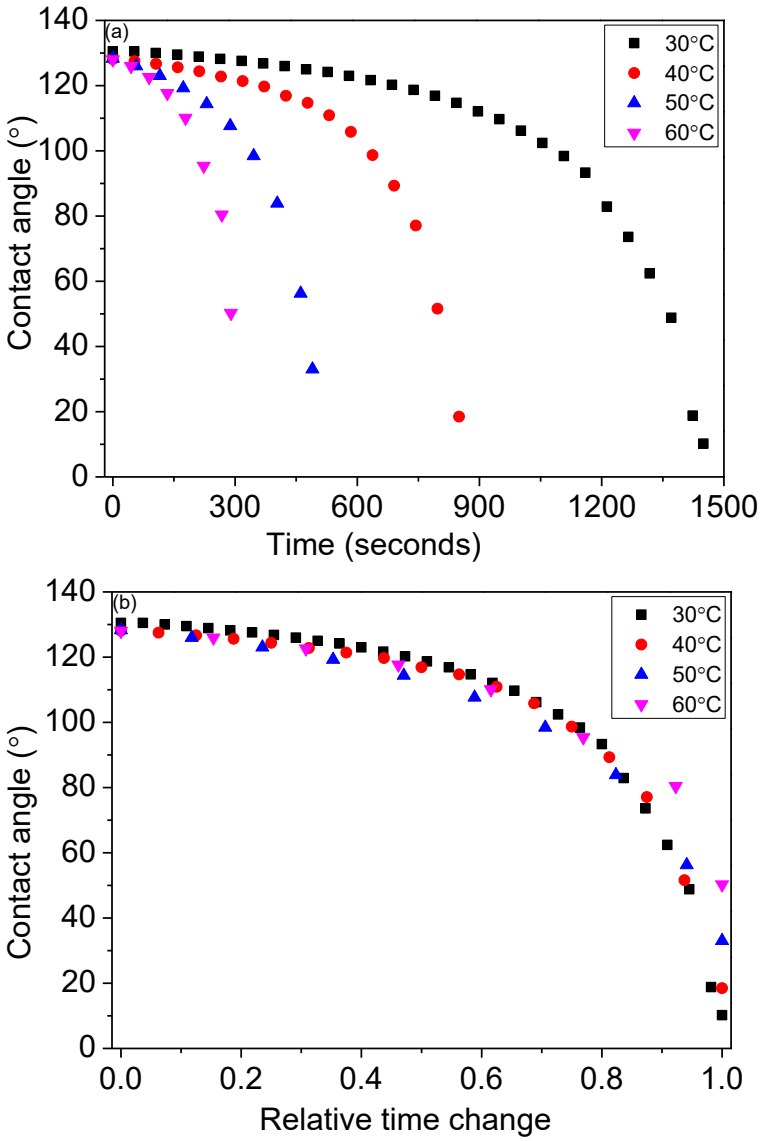

Figure 4 (a) Evolution of droplet contact angle during evaporation at different GDL temperatures (b) Relative time change of the droplet at different temperature.

At each initial GDL temperature, the contact angle of the droplet remains quite steady during the initial evaporation period, before decreasing more rapidly with the shrinking of the droplet, identified by a reduction in droplet diameter (Figure 5a). Taking the evaporation process at 30 ^{o}C as an example, the contact angle decreased from 130º to 110º at the initial stage (0 – 850 s), a decrease rate of 0.02º s^{-1}. This is followed by a transition (850 – 1150 s) where the contact angle reduced from 110º to 95º, a reduction rate of 0.05º s^{-1}. The evaporation process ends with a steep drop in the contact angle from 95º to 10º with a reduction rate of 0.24º s^{-1}. This would indicate that there are three regions in the evaporation dynamics of water droplets on a GDL in terms of contact angle. There is an initially low

reduction in contact angle due to the hydrophobic nature of the GDL preventing wetting of the surface. This is followed by a moderate reduction in the contact angle which indicates that the droplet is approaching the transition from non-wetting to wetting regime. This occurred at a contact angle of ~ 110º. This is in agreement with work done by Jinuntuya *et al.* [54] who studied the influence of wettability on liquid water transport in GDLs. Their model predicted that the transitioning into the wetting regime occurs between 100º and 120º. The final region in the evaporation process occurs when the transition to the wetting regime, which occurs by definition at 90º [55], after which the droplet rapidly evaporates. The droplet diameter can be seen to reduce steadily during evaporation (Figure 5a).

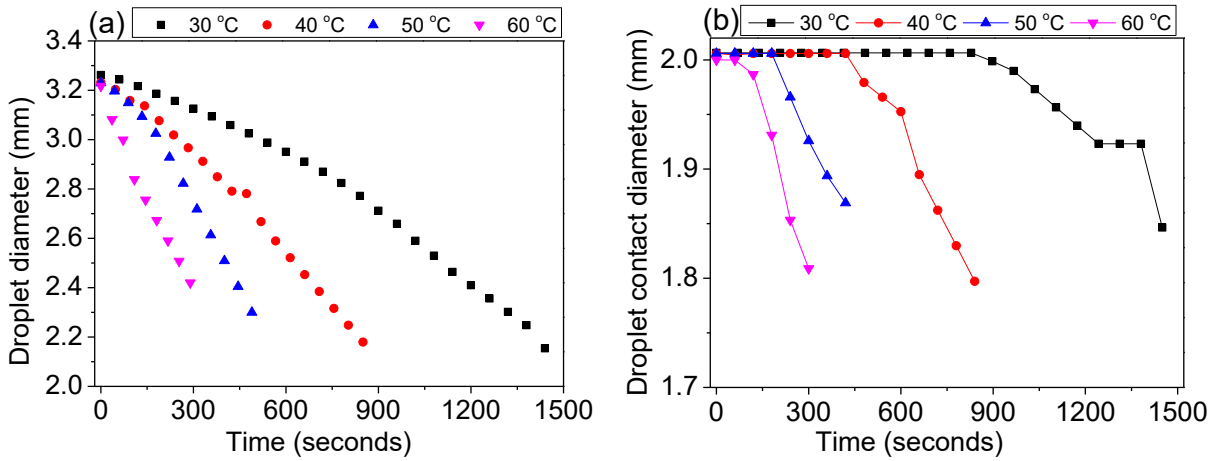

Figure 5 Evolution of droplet during evaporation at different GDL temperatures: (a) droplet diameter, (b) contact diameter.

The result from Figure 5b shows the contact diameter of the droplet is initially constant before decreasing. The contact diameter of the droplet is the contact line the droplet makes with the GDL. This is different from the droplet diameter, which is the width of the droplet itself. The reduction in the contact diameter is aligned with the transition in contact angle from non-wetting to wetting regime. This would indicate that when deciding materials for PEFC GDLs, a material that keeps the droplet pinned for a longer period of time will be advantageous as it will hinder flooding of the GDL. This is in agreement with work done by Fei *et al.* [33], Dash *et al.* [35] and McHale *et al.* [34] on droplet evaporation on hydrophobic and superhydrophobic surfaces. The initially fixed contact diameter of the droplet also indicates that droplet evaporation on GDLs proceeds in a pinned contact area mode, followed by a contact line retreat, which is in agreement with work done by McHale *et al.* [34], who studied liquid evaporation on superhydrophobic surfaces. It also agrees with work done by Zachary *et al.* [8] who identified droplet pinning on GDL surfaces during evaporation and also revealed that the strength of the pinning is dependent on the GDL material.

3.2 Thermal characterisation of water droplets on GDL

To better understand water droplet evaporation on a GDL, thermal characterisation was performed. This is particularly important as thermal imaging is being increasingly used for fuel cell diagnostics and the characterisation performed will help interpretation of droplet shape and form from infrared measurements.

3.2.1 GDL thermal characterisation

Before the thermal characterisation of the droplet on the GDL, the GDL itself was characterised in order to acquire a thermal image baseline. The emissivity of the GDL was obtained to be 0.97 by comparing the temperature reported by the camera with that of an imbedded thermocouple over a range of temperatures. The infrared camera was used to obtain temperature readings across a 1.4 cm line-scan (Figure 6a) with a pixel resolution of 100 × 100 μm. There are consistent distinct regions of high and low 'temperature', (e.g., high temperature at 1.05 cm and low temperature at 0.45 cm) which are exacerbated as the mean temperature increases. The statistical temperature distribution on the GDL surface (Figure 6b) also shows that as temperature increases the variance in the temperature measurement becomes larger.

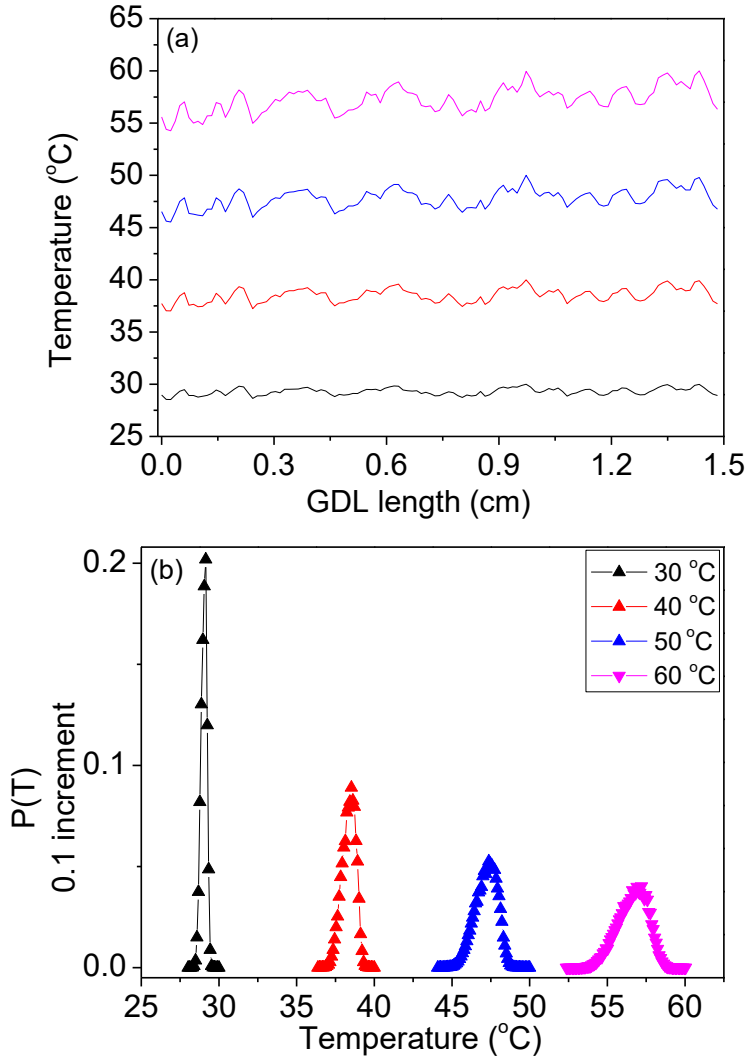

Figure 6 (a) Temperature distribution at different nominal temperatures along a single 1.4 cm line-scan on the GDL; (b) Statistical temperature distribution on 9 cm^2 GDL surface.

As emissivity variations on a sample influence the reported temperature from IR thermography, the structure of the GDL in relation to the pixel size needs to be characterised. Figure 6(b-c) shows the area associated with each pixel size based on a scanning electron micrograph and an X-ray CT image of the surface of the GDL. The pixel area during thermal imaging (Figure 6a) of the GDL is 100 × 100 µm. It is clearly seen that depending on the area examined, the observed 'depth' or geometry of the GDL varies, which can lead to change in emissivity. For example, Deloye *et al.* [56] showed that the emissivity of quartz sand varied by 5% depending on the surface composition, particle distribution and viewing angle. In order to examine if the observed variation in temperature is an emissivity effect, the Stefan-Boltzmann equation (Equation 1) is used to determine how much variation in reported temperature is linked to variation in emissivity.

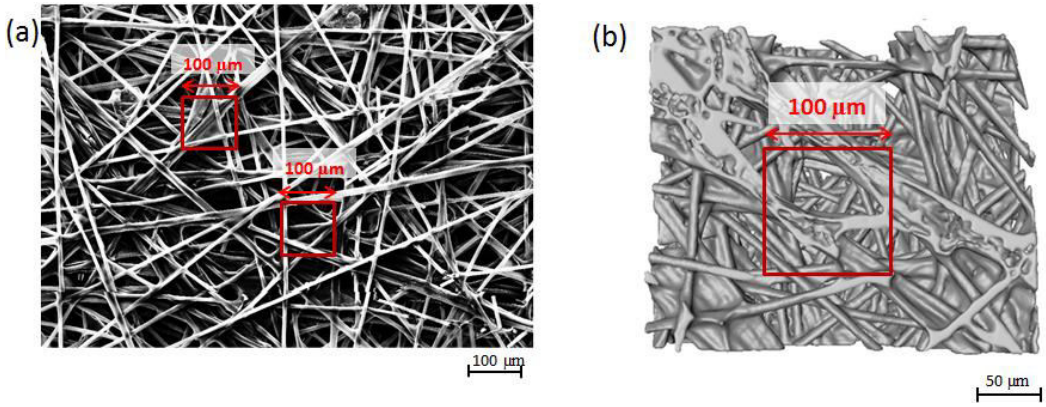

Figure 7 (a) Scanning electron micrograph of GDL with representative square sections showing the equivalent pixel size from the IR camera; (b) X-ray CT of GDL (top view) with pixel size represented.

The Stefan-Boltzmann equation (Equation 1) links the amount of energy radiated by a black body to the reported temperature and emissivity.

$$J^* = \varepsilon\sigma T^4 \qquad \text{Equation 1}$$

Where J^* is the total energy radiated per unit surface of area of a black body across all wavelengths per unit time, ε is the emissivity, σ is the Stefan-Boltzmann constant and T is the temperature in Kelvin. The effect a change in emissivity has on the reported temperature can be estimated from Equation **2**.

$$T \propto \sqrt[4]{1/\varepsilon} \qquad \text{Equation 2}$$

Assuming the actual emissivity of the different regions does not change with temperature, we can expect to see a $\frac{1}{T^4}$ dependence associated with the observed temperature spreading effect (Figure 6b). This is shown in Figure 8 which shows the variation in temperature observed in Figure 6b compared to the expected variation based on range of emissivity (80 – 95%). This range of emissivity was used for comparison as the likely emissivity change as a result of the different materials / geometries on the GDL should between these ranges.

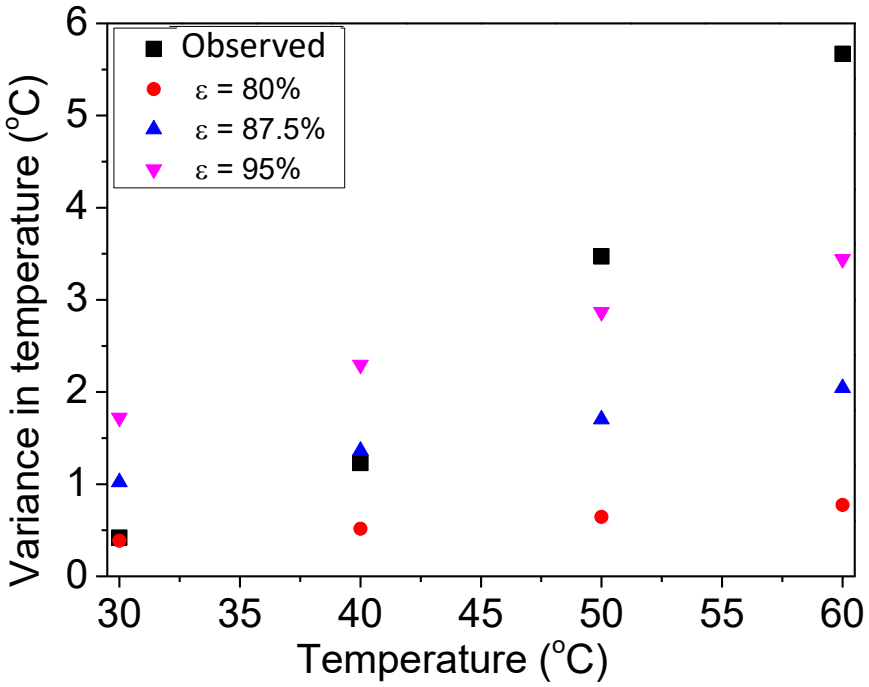

Figure 8 Comparison of observed experimental variation in GDL temperature over a 9 cm^2 area (Figure 6b) to the expected theoretical variations associated with different emissivity.

The result from Figure 8 indicates that emissivity is not the only reason for the observed temperature variation, as the associated temperature change observed is not consistent with the temperature over a range of emissivity. This would indicate that thermal gradients exists across the GDL despite its relatively small thickness and this has been observed and reported in other studies [57,58]; thermocouples were used, which provided temperature of the hotter active layer and the cooler GDL. However, this result shows that during thermal imaging, pixel resolution can uncover a range of temperatures from different depths in the GDL. Examining the SEM and X-ray CT images from Figure 6 (b-c), it is seen that the GDL has a highly non-uniform surface and the pixel area across will sample different depths into the sample. This would explain the consistent temperature profiles (peaks and troughs observed) in the linear profiles taken from the thermal images (Figure 6a), which got exacerbated as the GDL temperature increased as a result of the increased thermal gradients.

3.2.2 Droplet thermal characterisation

With the GDL characterisation complete and baseline temperature profiles obtained, 8 µl droplets were introduced onto the controlled temperature GDL using a syringe (Figure 9). Droplet evaporation was detected visually with the disappearance of the droplet and a rise in the local temperature of the area where the droplet resided.

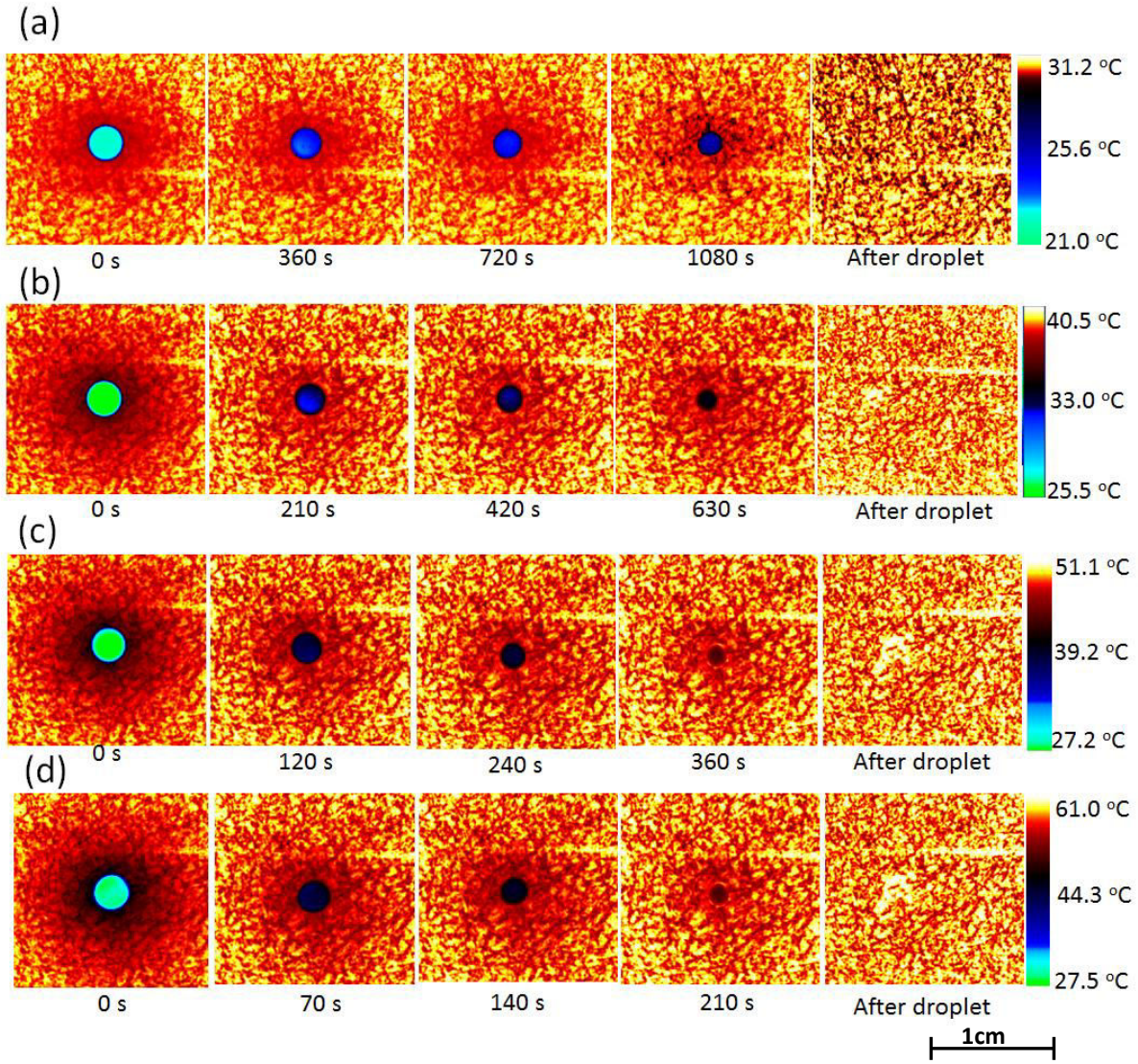

Figure 9 Thermal imaging of water droplet on GDL at a range of set temperatures: (a) 30 °C, (b) 40 °C, (c) 50 °C and (d) 60 °C.

In the images, the circular profile of the droplet at a lower temperature than the GDL is very well defined; a 'halo effect' is also noticeable whereby the droplet has a cooling effect on the surrounding GDL area. The subtle line seen in Figure 9 is as a result of a possible microscopic scratch on the GDL which is not visible to the naked eye. The associated lower temperature is due to the fact that the camera is likely to be measuring infrared from a slightly deeper portion of the GDL. This made no difference to the results as the temperature difference between the scratched surface and the normal surface of the GDL (without the droplet) is less than 1°C.

Figure 10a shows the temperature at the centre of the droplet with time. On initial contact with the GDL, the droplet rapidly increases in temperature and reaches a characteristic plateau temperature. This plateau temperature is independent of the initial starting

temperature of the water droplet and represents an equilibrium temperature that is a balance between the heating effect of the GDL and the cooling effect of evaporation, as shown in Figure 10b.

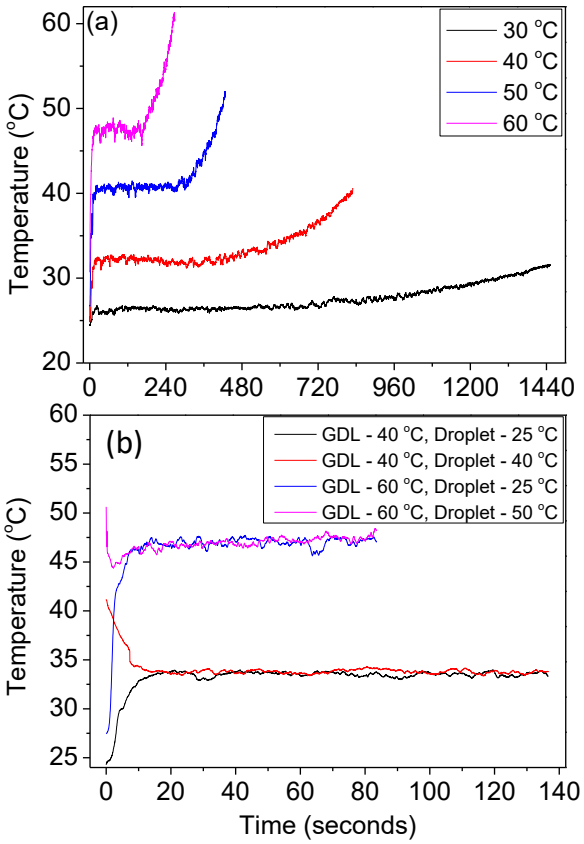

Figure 10 (a) Evolution of temperature of the centre of the droplet during evaporation; (b) comparison of droplet evaporation profile at different initial droplet temperatures

The difference in measured temperature is not a consequence of emissivity differences, as water has an emissivity of 0.95, while the GDL has an emissivity of 0.97, which should lead to a temperature difference of only ~ 0.4 ºC, based on Equation 2. Following the plateau region, the onset of temperature increase coincides with the transition into the wetting regime, as shown in Figure 5a. This shows that thermal characterisation can be used to identify the transition from non-wetting to wetting regime of droplets on hydrophobic surfaces. While the centre temperature provides useful information about evaporation dynamics, a full temperature profile across the droplet and surrounding area is necessary for understanding the cooling effect on the GDL and how to interpret the IR profiles of water droplets in operational fuel cells. The temperature profile of the entire droplet during evaporation at a GDL temperature of 30 ºC is shown in Figure 11a, while the profile of the droplet and surround GDL is shown in Figure 11b. The pixel resolution was 100 µm. The evaporation of the droplet is clearly displayed in Figure 11a with the reduction in its diameter

from 3.5 mm at 0 seconds to 2.3 mm at 1080 seconds. This is in close agreement to the drop analysis performed earlier (Figure 5b), where an initial droplet diameter of 3.3 mm was obtained and the droplet diameter at 1080 s was ~ 2.3 mm.

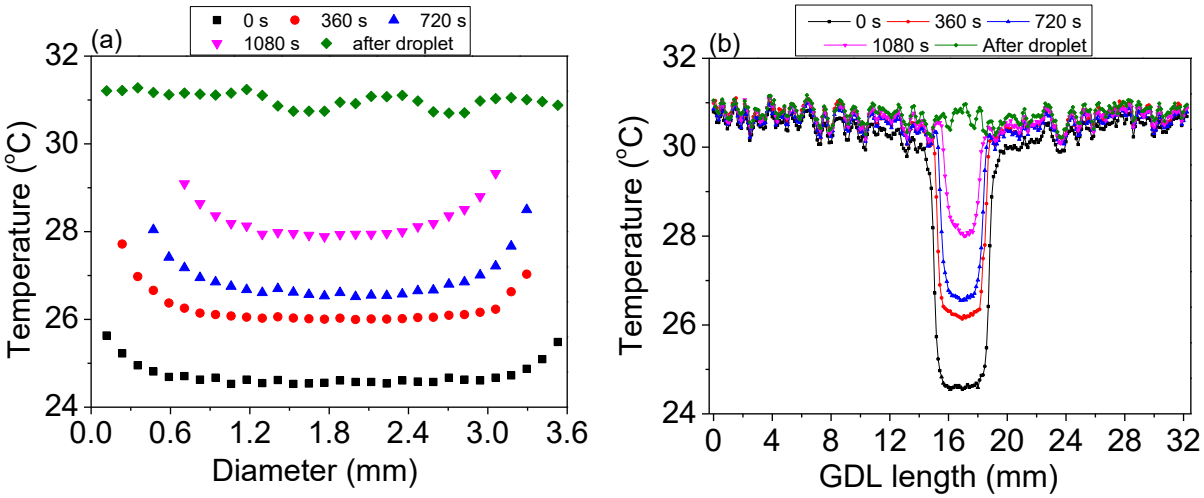

Figure 11 Spatial temperature profile of (a) water droplet and (b) droplet and surrounding GDL at 30 ºC

There was also a ~ 1 ºC reported difference in temperature between the edges of the droplet and its centre. This could be as a result of the edges benefiting from a higher heat transfer from the surrounding GDL than the centre. However, without the initial wettability calibration, the actual diameter of the droplet could have been over estimated, as the 'halo' effect extends the cooling region out to as much as 5 mm from the centre of the droplet (Figure 10). The effect is exacerbated as the GDL temperature increases due to the higher difference in temperature between the droplet and the GDL.

4. Conclusion

Water droplet evaporation dynamics on a heated GDL has been studied *ex situ* using wettability analysis and thermal characterisation. Evaporation dynamics show a transition from non-wetting to wetting with minimal change in the droplets' contact diameter until the transition contact angle is attained, while there is a constant reduction in the droplet diameter until evaporation.

Thermal imaging has also been used as an effective tool for the characterisation of the thermal effect of water droplets. This work also reveals that non-uniformity in GDL structure leads to a variation in reported temperature when using an infrared camera as a result of thermal gradients and unlevelled surface (porous structure on same scale as image resolution)

of the GDL. Cooling profiles exist around droplets due to the so-called halo effect; this should not be mistaken for a droplet while using an infrared camera.

Acknowledgments

The authors would like to acknowledge Sunshine Oil and Chemical Development Company Limited for supporting Obeisun's Ph.D. scholarship and the National Physical Laboratory for supporting Finegan and Engebretsen. The EPSRC is acknowledged for funding the Electrochemical Innovation Lab's fuel cell research programme through (EP/K038656/1; EP/G060991/1; EP/J001007/1; EP/I037024/1; EP/G030995/1; EP/G04483X/1). PRS acknowledges the Royal Academy of Engineering for funding support.

References

[1] Obeisun OA, Meyer Q, Robinson J, Gibbs CW, Kucernak AR, Shearing PR, et al. Development of open-cathode polymer electrolyte fuel cells using printed circuit board flow-field plates: Flow geometry characterisation. Int J Hydrogen Energy 2014;39:18326–36. doi:10.1016/j.ijhydene.2014.08.106.

[2] Obeisun OA, Meyer Q, Gibbs CW, Robinson JB, Shearing PR, Bret. Advanced diagnostics applied to a self-breathing fuel cell. ECS Trans 2014;61:249–58.

[3] Jeong SU, Cho EA, Kim H-J, Lim T-H, Oh I-H, Kim SH. Effects of cathode open area and relative humidity on the performance of air-breathing polymer electrolyte membrane fuel cells. J Power Sources 2006;158:348–53. doi:10.1016/j.jpowsour.2005.09.044.

[4] Ying W, Ke J, Lee W, Yang T, Kim C. Effects of cathode channel configurations on the performance of an air-breathing PEMFC. Int J Hydrogen Energy 2005;30:1351–61. doi:10.1016/j.ijhydene.2005.04.009.

[5] Burheim OS, Ellila G, Fairweather JD, Labouriau a., Kjelstrup S, Pharoah JG. Ageing and thermal conductivity of Porous Transport Layers used for PEM Fuel Cells. J Power Sources 2013;221:356–65. doi:10.1016/j.jpowsour.2012.08.027.

[6] Gurau V, Bluemle MJ, De Castro ES, Tsou Y-M, Mann JA, Zawodzinski T a. Characterization of transport properties in gas diffusion layers for proton exchange membrane fuel cells. J Power Sources 2006;160:1156–62. doi:10.1016/j.jpowsour.2006.03.016.

[7] Bazylak A, Sinton D, Djilali N. Dynamic water transport and droplet emergence in PEMFC gas diffusion layers. J Power Sources 2008;176:240–6. doi:10.1016/j.jpowsour.2007.10.066.

[8] Fishman JZ, Leung H, Bazylak a. Droplet pinning by PEM fuel cell GDL surfaces. Int J Hydrogen Energy 2010;35:9144–50. doi:10.1016/j.ijhydene.2010.06.027.

[9] Perrin J-C, Lyonnard S, Guillermo A, Levitz P. Water dynamics in ionomer membranes by field-cycling NMR relaxometry. Magn Reson Imaging 2007;25:501–4. doi:10.1016/j.mri.2007.01.002.

[10] Dunbar Z, Masel RI. Quantitative MRI study of water distribution during operation of a PEM fuel cell using Teflon® flow fields. J Power Sources 2007;171:678–87. doi:10.1016/j.jpowsour.2007.06.207.

[11] Feindel KW, Bergens SH, Wasylishen RE. Use of hydrogen–deuterium exchange for contrast in 1H NMR microscopy investigations of an operating PEM fuel cell. J Power Sources 2007;173:86–95. doi:10.1016/j.jpowsour.2007.04.079.

[12] Hartnig C, Manke I, Kardjilov N, Hilger a., Grünerbel M, Kaczerowski J, et al. Combined neutron radiography and locally resolved current density measurements of operating PEM fuel cells. J Power Sources 2008;176:452–9. doi:10.1016/j.jpowsour.2007.08.058.

[13] Owejan JP, Gagliardo JJ, Sergi JM, Kandlikar SG, Trabold T a. Water management studies in PEM fuel cells, Part I: Fuel cell design and in situ water distributions. Int J Hydrogen Energy 2009;34:3436–44. doi:10.1016/j.ijhydene.2008.12.100.

[14] Gebel G, Diat O, Escribano S, Mosdale R. Water profile determination in a running PEMFC by small-angle neutron scattering. J Power Sources 2008;179:132–9. doi:10.1016/j.jpowsour.2007.12.124.

[15] Chen Y-S, Peng H, Hussey DS, Jacobson DL, Tran DT, Abdel-Baset T, et al. Water distribution measurement for a PEMFC through neutron radiography. J Power Sources 2007;170:376–86. doi:10.1016/j.jpowsour.2007.03.076.

[16] Owejan JP, Trabold T a., Gagliardo JJ, Jacobson DL, Carter RN, Hussey DS, et al. Voltage instability in a simulated fuel cell stack correlated to cathode water accumulation. J Power Sources 2007;171:626–33. doi:10.1016/j.jpowsour.2007.06.174.

[17] Isopo A, Rossi Albertini V. An original laboratory X-ray diffraction method for in situ investigations on the water dynamics in a fuel cell proton exchange membrane. J Power Sources 2008;184:23–8. doi:10.1016/j.jpowsour.2008.06.046.

[18] Lee SJ, Lim N-Y, Kim S, Park G-G, Kim C-S. X-ray imaging of water distribution in a polymer electrolyte fuel cell. J Power Sources 2008;185:867–70. doi:10.1016/j.jpowsour.2008.08.101.

[19] Sinha PK, Halleck P, Wang C-Y. Quantification of Liquid Water Saturation in a PEM Fuel Cell Diffusion Medium Using X-ray Microtomography. Electrochem Solid-State Lett

2006;9:A344. doi:10.1149/1.2203307.

[20] Spernjak D, Prasad AK, Advani SG. Experimental investigation of liquid water formation and transport in a transparent single-serpentine PEM fuel cell. J Power Sources 2007;170:334–44. doi:10.1016/j.jpowsour.2007.04.020.

[21] Tüber K, Pócza D, Hebling C. Visualization of water buildup in the cathode of a transparent PEM fuel cell. J Power Sources 2003;124:403–14. doi:10.1016/S0378-7753(03)00797-3.

[22] Zhang FY, Yang XG, Wang CY. Liquid Water Removal from a Polymer Electrolyte Fuel Cell. J Electrochem Soc 2006;153:A225. doi:10.1149/1.2138675.

[23] Liu X, Guo H, Ma C. Water flooding and two-phase flow in cathode channels of proton exchange membrane fuel cells. J Power Sources 2006;156:267–80. doi:10.1016/j.jpowsour.2005.06.027.

[24] Liu X, Guo H, Ye F, Ma CF. Water flooding and pressure drop characteristics in flow channels of proton exchange membrane fuel cells. Electrochim Acta 2007;52:3607–14. doi:10.1016/j.electacta.2006.10.030.

[25] Ge S, Wang C-Y. Liquid Water Formation and Transport in the PEFC Anode. J Electrochem Soc 2007;154:B998. doi:10.1149/1.2761830.

[26] Kim H-S, Min K. Experimental investigation of dynamic responses of a transparent PEM fuel cell to step changes in cell current density with operating temperature. J Mech Sci Technol 2009;22:2274–85. doi:10.1007/s12206-008-0702-4.

[27] Mortazavi M, Tajiri K. Effect of the PTFE content in the gas diffusion layer on water transport in polymer electrolyte fuel cells (PEFCs). J Power Sources 2014;245:236–44. doi:10.1016/j.jpowsour.2013.06.138.

[28] Meyer Q, Ronaszegi K, Pei-June G, Curnick O, Ashton S, Reisch T, et al. Optimisation of air cooled, open-cathode fuel cells: Current of lowest resistance and electro-thermal performance mapping. J Power Sources 2015;291:261–9. doi:10.1016/j.jpowsour.2015.04.101.

[29] Birdi KS, Vu DT. Wettability and the evaporation rates of fluids from solid surfaces. J Adhes Sci Technol 1993;7:485–93. doi:10.1163/156856193X00808.

[30] Kulinich SA, Farzaneh M. Effect of contact angle hysteresis on water droplet evaporation from super-hydrophobic surfaces. Appl Surf Sci 2009;255:4056–60. doi:10.1016/j.apsusc.2008.10.109.

[31] Anantharaju N, Panchagnula M, Neti S. Evaporating drops on patterned surfaces: transition from pinned to moving triple line. J Colloid Interface Sci 2009;337:176–82. doi:10.1016/j.jcis.2009.04.095.

[32] G. Picknett RB. The Evaporation of Sessile or Pendant Drops in Still Air. J Colloid Interface Sci 1977;61:336–50.

[33] Hao P, Lv C, He F. Evaporating behaviors of water droplet on superhydrophobic surface. Sci China Physics, Mech Astron 2012;55:2463–8. doi:10.1007/s11433-012-4940-1.

[34] Mchale G, Aqil S, Shirtcliffe NJ, Newton MI, Erbil HY. Analysis of Droplet Evaporation on a Superhydrophobic Surface 2005:11053–60.

[35] Dash S, Garimella S V. Droplet evaporation on heated hydrophobic and superhydrophobic surfaces. Phys Rev E 2014;89:042402. doi:10.1103/PhysRevE.89.042402.

[36] Shimoi R, Masuda M, Fushinobu K, Kozawa Y, Okazaki K. Visualization of the Membrane Temperature Field of a Polymer Electrolyte Fuel Cell. J Energy Resour Technol 2004;126:258. doi:10.1115/1.1811119.

[37] Hakenjos A, Muenter H, Wittstadt U, Hebling C. A PEM fuel cell for combined measurement of current and temperature distribution, and flow field flooding. J Power Sources 2004;131:213–6. doi:10.1016/j.jpowsour.2003.11.081.

[38] Brett DJL, Aguiar P, Clague R, Marquis a. J, Schöttl S, Simpson R, et al. Application of infrared thermal imaging to the study of pellet solid oxide fuel cells. J Power Sources 2007;166:112–9. doi:10.1016/j.jpowsour.2006.12.098.

[39] Wang M, Guo H, Ma C. Temperature distribution on the MEA surface of a PEMFC with serpentine channel flow bed. J Power Sources 2006;157:181–7. doi:10.1016/j.jpowsour.2005.08.012.

[40] Noorkami M, Robinson JB, Meyer Q, Obeisun OA, Fraga ES, Reisch T, et al. Effect of temperature uncertainty on polymer electrolyte fuel cell performance. Int J Hydrogen Energy 2014;39:1439–48. doi:10.1016/j.ijhydene.2013.10.156.

[41] Meyer Q, Ashton S, Curnick O, Reisch T, Adcock P, Ronaszegi K, et al. Dead-Ended Anode Polymer Electrolyte Fuel Cell Stack Operation Investigated using Electrochemical Impedance Spectroscopy, Off-gas Analysis and Thermal Imaging. J Power Sources 2013;254:1–9. doi:10.1016/j.jpowsour.2013.11.125.

[42] Burheim OS, Su H, Hauge HH, Pasupathi S, Pollet BG. Study of thermal conductivity of PEM fuel cell catalyst layers. Int J Hydrogen Energy 2014;39:9397–408. doi:10.1016/j.ijhydene.2014.03.206.

[43] Burheim OS, Pharoah JG, Lampert H, Vie PJS, Kjelstrup S. Through-Plane Thermal Conductivity of PEMFC Porous Transport Layers. J Fuel Cell Sci Technol 2011;8:021013. doi:10.1115/1.4002403.

[44] Knights SD, Colbow KM, St-Pierre J, Wilkinson DP. Aging mechanisms and lifetime of PEFC and DMFC. J Power Sources 2004;127:127–34. doi:10.1016/j.jpowsour.2003.09.033.

[45] Zhang G, Kandlikar SG. A critical review of cooling techniques in proton exchange membrane fuel cell stacks. Int J Hydrogen Energy 2012;37:2412–29. doi:10.1016/j.ijhydene.2011.11.010.

[46] Chen FC, Gao Z, Loutfy RO, Hecht M. Analysis of Optimal Heat Transfer in a PEM Fuel Cell Cooling Plate. Fuel Cells 2003;3:181–8. doi:10.1002/fuce.200330112.

[47] Flückiger R, Tiefenauer A, Ruge M, Aebi C, Wokaun A, Büchi FN. Thermal analysis and optimization of a portable, edge-air-cooled PEFC stack. J Power Sources 2007;172:324–33. doi:10.1016/j.jpowsour.2007.05.079.

[48] Lasbet Y, Auvity B, Castelain C, Peerhossaini H. A chaotic heat-exchanger for PEMFC cooling applications. J Power Sources 2006;156:114–8. doi:10.1016/j.jpowsour.2005.08.030.

[49] Yuan Y, Lee TR. Surface Science Techniques. vol. 51. Berlin, Heidelberg: Springer Berlin Heidelberg; 2013. doi:10.1007/978-3-642-34243-1.

[50] Das PK, Grippin A, Kwong A, Weber AZ. Liquid-Water-Droplet Adhesion-Force Measurements on Fresh and Aged Fuel-Cell Gas-Diffusion Layers. J Electrochem Soc 2012;159:B489. doi:10.1149/2.052205jes.

[51] Cooper SJ, Eastwood DS, Gelb J, Damblanc G, Brett DJL, Bradley RS, et al. Image based modelling of microstructural heterogeneity in LiFePO4 electrodes for Li-ion batteries. J Power Sources 2013.

[52] Chandra S, Marzo M, Qiao YM, Tartarini P. Effect of Liquid-Solid Contact Angle on Droplet Evaporation 1997;27:141–58.

[53] Lim C, Wang CY. Effects of hydrophobic polymer content in GDL on power performance of a PEM fuel cell. Electrochim Acta 2004;49:4149–56. doi:10.1016/j.electacta.2004.04.009.

[54] Jinuntuya F, Chen R, Ostadi H. The Effects of Wettability on Liquid Water Transport in Gas Diffusion Layers using Lattice Boltzmann Method. n.d.

[55] Grundke K, Pöschel K, Synytska a, Frenzel R, Drechsler a, Nitschke M, et al. Experimental studies of contact angle hysteresis phenomena on polymer surfaces - Toward the understanding and control of wettability for different applications. Adv Colloid Interface Sci 2014:1–27. doi:10.1016/j.cis.2014.10.012.

[56] Deloye CJ, West MS, Grossmann JM. Changes in apparent emissivity as a function of viewing geometry. Int Soc Opt Eng 2011;8040:80400J – 80400J – 12. doi:10.1117/12.887737.

[57] Straubhaar B, Pauchet J, Prat M. Water transport in gas diffusion layer of a polymer electrolyte fuel cell in the presence of a temperature gradient. Phase change effect. Int J Hydrogen Energy

2015:2–9. doi:10.1016/j.ijhydene.2015.04.027.

[58] Thomas A, Maranzana G, Didierjean S, Dillet J, Lottin O. Thermal and water transfer in PEMFCs: Investigating the role of the microporous layer. Int J Hydrogen Energy 2014;39:2649–58. doi:10.1016/j.ijhydene.2013.11.105.